Direct-Current Induced Dynamics in $Co_{90}Fe_{10}/Ni_{80}Fe_{20}$ Point Contacts

W. H. Rippard, M. R. Pufall, S. Kaka, S. E. Russek, and T. J. Silva
National Institute of Standards and Technology, Boulder, Colorado 80305, USA
(Received 23 June 2003; published 15 January 2004)

We have directly measured coherent high-frequency magnetization dynamics in ferromagnetic films induced by a spin-polarized dc current. The precession frequency can be tuned over a range of several gigahertz by varying the applied current. The frequencies of excitation also vary with applied field, resulting in a microwave oscillator that can be tuned from below 5 to above 40 GHz. This novel method of inducing high-frequency dynamics yields oscillations having quality factors from 200 to 800. We compare our results with those from single-domain simulations of current-induced dynamics.

DOI: 10.1103/PhysRevLett.92.027201 PACS numbers: 75.47.–m, 75.75.+a, 85.75.–d

Since the initial predictions of Slonczewski [1] and Berger [2] that a spin-polarized current can induce magnetic switching and dynamic excitations in ferromagnetic thin films, a great deal of work has focused on understanding the interactions between polarized currents and ferromagnetic nanostructures [3]. It was predicted, and later confirmed, that this effect can lead to current-controlled hysteretic switching in magnetic nanostructures in moderate applied magnetic fields [4,5]. This behavior is not only of scientific interest but also finds potential applications in devices such as current-controlled switching of magnetic random access memory elements and has implications for the stability of magnetic hard-disk read heads. Another prediction is that the spin torque can drive steady-state magnetization precession in the case of applied fields large enough to oppose hysteretic switching [1,2]. Numerous applications exist for such current-controlled microwave oscillators that are integrable with semiconductor electronics [6]. However, with one recent exception in nanopillar devices [7], to date no direct measurements of these high-frequency dynamics have been reported [4,5,8]. Here we report direct measurements of spin-torque induced magnetization dynamics for in-plane and out-of-plane applied fields as a function of field strength H and current I, and compare the results with simulations based on the theoretical model of Ref. [1].

Studies discussed here were performed on lithographically defined point contacts to spin valve mesas ($8\ \mu m \times 12\ \mu m$). The point contacts are nominally 40 nm diameter circles, have resistances between 4 and 10 Ω, and show no indications of tunneling in their transport characteristics. Top and bottom electrical contacts to the devices are patterned into 50 Ω planar waveguides. Fabrication details will be presented elsewhere. Specifically, the spin valve structures are Ta (2.5 nm)/Cu (50 nm)/$Co_{90}Fe_{10}$ (20 nm)/Cu (5 nm)/$Ni_{80}Fe_{20}$ (5 nm)/Cu (1.5 nm)/Au (2.5 nm) and show typical magnetoresistance (MR) values of 80 mΩ. The $Co_{90}Fe_{10}$ is the "fixed" layer in terms of the spin torque due to its larger volume, exchange stiffness, and saturation magnetization compared with $Ni_{80}Fe_{20}$ [9]. The device is contacted with microwave probes and a dc current is injected through a bias-tee, along with a 20 μA ac current (500 Hz), allowing simultaneous measurement of the dc resistance, differential resistance, and microwave output. The devices are current biased so that changes in the alignment between the $Ni_{80}Fe_{20}$ and $Co_{90}Fe_{10}$ layers appear as voltage changes across the point contact. The high-frequency voltage signal is measured with either a 50 GHz spectrum analyzer or a 1.5 GHz real-time oscilloscope. The bandwidth of the circuit is 0.1 to 40 GHz. Measurements were performed at room temperature. All results discussed here occur for only one direction of current, corresponding to electrons flowing from the top contact into the spin valve.

Figure 1(a) shows a differential resistance dV/dI curve of a device taken with an in-plane field $\mu_0 H = 0.1$ T. The nonhysteretic peak in the dV/dI curve, at $I = 4$ mA in Fig. 1(a), has been taken as indirect evidence of current-induced magnetization dynamics [4,5,8]. Tsoi *et al.* demonstrated changes in the dc transport properties of point contacts under the influence of external radiation, implying a relationship between spin dynamics and dc resistance [8]. Here we observe these dynamics directly, as shown in Fig. 1(b). For low currents, no peaks are observed in the spectra. As I is increased to 4 mA a peak appears at $f = 7.9$ GHz. As I is further increased, the peak frequency decreases, a trend observed for all in-plane fields measured. This frequency redshift is linear in I (inset) and typically varies from ≈ 0.2 GHz/mA at low fields (≈ 50 mT) to ≈ 1 GHz/mA at fields of ≈ 0.8 T. At higher values of I, the excitations decrease in magnitude until no peaks are observed, as shown in the $I = 9$ mA spectrum. Assuming the high-frequency signals result from a MR response, we estimate a maximum excursion angle between the layers of approximately 20°. As the measured peak amplitude does not increase linearly with I (as it would for fixed excursion angle), we infer that the orbit traversed by the magnetization changes with I. The dynamics here are strongly correlated with the peak in the dV/dI curve. This is not the case for all devices:

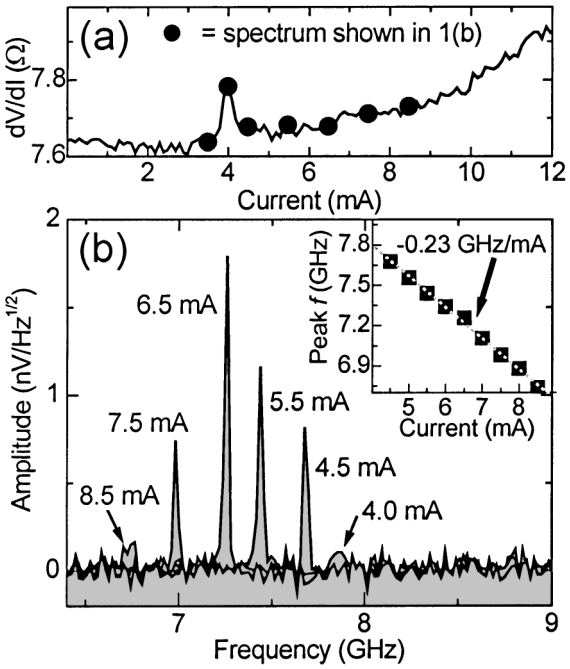

FIG. 1. (a) dV/dI vs I with $\mu_0 H = 0.1$ T. (b) High frequency spectra taken at several different values of current through the device, corresponding to the symbols in (a). Variation of f with I (inset).

Typically the onset of the dynamics occurs only in the vicinity of a feature (step, peak, or kink) in dV/dI, and the relative position of this onset varies with H.

To better understand the possible trajectories of these excitations, we compare our results with simulations that assume an isolated single-domain particle (40 nm × 40 nm) whose behavior is described by a modified Landau-Lifshitz-Gilbert (LLG) equation proposed by Slonczewski [1]. This only approximates the point contact geometry, where the region undergoing dynamic excitations is coupled to a continuous film by intralayer exchange. For example, effects associated with the formation of domain walls between the region under the contact area and the rest of the free layer are not included, nor are effects of spin-wave radiation damping [1]. Finite-temperature effects are included through a randomly fluctuating field [10].

The simulations show two basic regimes of motion for in-plane fields. At low current, when oscillations begin, the magnetization $\boldsymbol{M}$ precesses in a nearly elliptical mode about $\boldsymbol{H}$ and the time-averaged magnetization $\langle \boldsymbol{M} \rangle$ lies parallel to $\boldsymbol{H}$. As I increases, the trajectories become nonelliptical and have greater excursion angles with respect to $\boldsymbol{H}$. However, $\boldsymbol{M}$ continues to precess about the applied field, while $\langle \boldsymbol{M} \rangle$ changes from parallel to antiparallel alignment with $\boldsymbol{H}$. Within this regime, the simulated excitation frequency *decreases* approximately linearly with I, in agreement with the data shown in Fig. 1(b). Furthermore, $|df/dI|$ increases with increasing H, also in agreement with our measurements. As I is further increased, the second regime is reached and the simulations show $\boldsymbol{M}$ precessing out-of-plane with the precession frequency *increasing* with current. Consequently, we infer that the observed excitations correspond only to in-plane precession, perhaps due to a lack of stability of the trajectories in our devices, or because the devices are unable to support sufficient current densities. It may also indicate a need to incorporate micromagnetic effects in the modeling.

The measured linewidths are quite narrow, indicating that the excitations can be considered coherent single-mode oscillations. The peaks in Fig. 1(b) have full-width-at-half-maximum (FWHM) of ≈20 MHz and voltage (power) quality factors $Q = f/(\text{FWHM})$ of ≈350 (600), with particular values depending on I. The FWHMs of the excitations only weakly depend on H, leading to values of $Q > 500$ for $f > 30$ GHz. Analogous linewidths in ferromagnetic resonance (FMR) measurements would give damping parameters of $\alpha = 1\text{–}5 \times 10^{-4}$, with the particular value depending on H [11]. Our modeling requires $\alpha = 0.5\text{–}1 \times 10^{-3}$ to produce similar linewidths at 300 K. Either analysis gives values of α much smaller than values obtained through field-induced excitations of $Ni_{80}Fe_{20}$ thin films ($\alpha = 0.01$ to 0.005) [12,13]. Linewidths we have measured in nanopillar devices (not shown here) are about a factor of 5 larger than those measured in point contacts, showing that the narrowness of these peaks is not a general result for current-induced excitations. The lack of physical magnetic edges in point contact devices may account for their narrow linewidths in comparison to nanopillars. Increased linewidths and effective damping are often found in magnetic nanostructures, resulting from $\boldsymbol{M}$ at the edges of patterned devices lagging $\boldsymbol{M}$ at the center of the device during large-angle oscillations [13].

Figure 2(a) shows the measured frequencies as a function of in-plane field. The data correspond to the highest-frequency (lowest-current) excitation observed at a given H. Below $\mu_0 H = 50$ mT no excitations are seen. Around $\mu_0 H = 0.6$ T the excitation amplitude begins to drop and by $\mu_0 H > 1$ T is below our noise floor. The data are fit using the Kittel equation for in-plane magnon generation, excluding dipole effects, appropriate for the thin-film limit [14]:

$$f(H) = (g\mu_B\mu_0/h)[(H + H_{sw} + H_k + M_{\text{eff}}) \times (H + H_{sw} + H_k)]^{1/2}, \quad (1)$$

where $H_{sw} = Dk^2/(g\mu_B\mu_0)$, D is the exchange stiffness, g is the Landé factor, k is the magnon wave number, M_{eff} is the effective magnetization, H_k is the anisotropy field, μ_0 is the permeability of free space, h is Planck's constant, and μ_B is the Bohr magneton. In fitting the data, k and g are treated as free parameters while fixed values of $\mu_0 M_{\text{eff}} = 0.8$ T and $\mu_0 H_k = 0.4$ mT are used, as determined from magnetometry measurements. The fit

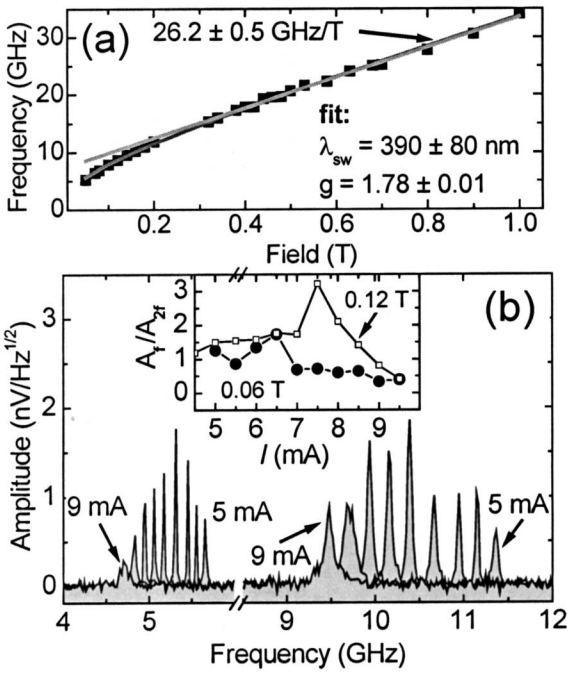

FIG. 2. (a) In-plane f vs H dispersion curve along with a fit to Eq. (1). Error bars (FWHM) are smaller than the data points. (b) Frequency spectra for $I = 5$ mA to 9 mA in 0.5 mA steps with $\mu H = 0.06$ T showing responses at both f and $2f$. (Inset) f to $2f$ amplitude ratios as a function of I for two different fields.

yields $g = 1.78 \pm 0.01$ and a magnon wavelength of $\lambda = 390 \pm 80$ nm. We note Eq. (1) is strictly valid only in the limit of small amplitude spin-waves, a limit not strictly met in the present measurements, as discussed above. From both the above fit and from the linear portion of the data for $\mu_0 H > 0.4$ T we determine $g = 1.78 \pm 0.01$, smaller than the value of $g = 2.0$ determined on analogous films by other methods [12,13]. However, numerical simulations of the LLG equation show that fitting Eq. (1) to oscillations of large amplitude results in an apparently suppressed value of g as found here. It was initially predicted that the lowest-order excited mode would have a wavelength of roughly twice the contact diameter [1]. However, the excitation wavelengths determined from fits to these and other data are much larger than the nominal or calculated contact sizes, which range from 25 to 40 nm from a Sharvin-Maxwell calculation [15]. We infer that the excitations are ones with negligible wave vector, i.e., the uniform FMR mode, although this does not exclude the presence of excitations outside our measurement bandwidth. Device-to-device variation of the measured f at a given H is $<10\%$, while the calculated contact size varies by 60%, consistent with the excitation of a long-wavelength mode.

Spectra taken over a wider range of frequencies show a peak at twice the frequency of the one discussed above as shown in Fig. 2(b). The frequencies, along with their variations with both I and H, differ by a factor of 2.00 ± 0.01, and are observed in fields much larger than any anisotropies in the film. We have not observed higher-harmonic signals. The ratios of the f to $2f$ amplitudes depend on both I and H, and show a nonmonotonic dependence on I and a slight increase with H (inset). For precession symmetric about the fixed layer direction, the signal from a MR-derived voltage should be twice the physical oscillation frequency of $\boldsymbol{M}$. However, any misalignment between the layers would result in the detection of a signal at f as well as $2f$. We estimate a misalignment of a few degrees would give the f to $2f$ amplitude ratios observed. The limiting slope of the data in Fig. 2(a) is 26 GHz/T, in good agreement with the value expected from Eq. (1) for a first harmonic signal, indicating that the lower-frequency peaks correspond to the physical precessional frequency of $\boldsymbol{M}$.

The devices also emit power at lower frequency. Figure 3 shows $I = 5$ mA and 11 mA spectra of the device along with the corresponding dV/dI curve. At low I, no signal is found, but as I is increased to 8 mA, a shoulder in the dV/dI curve appears and a signal is observed, the strength of which increases with current. In this device, by $I = 8$ mA the coherent dynamics discussed above have already turned off. However, we have measured other devices where both the high-frequency single-mode oscillations and the low-frequency signal have been simultaneously observed over a range of currents. From real-time measurements of the voltage fluctuations in these devices and nanopillars, we find that this low-frequency signal results from two-state switching in the device, as has also been reported in Ref. [5]. The spectral shape follows a Lorentzian function, as expected for stochastic switching between two well-defined energy states [16]. At higher currents this switching typically ceases, although this is not always the case before the highest I supported by a contact (≈ 14 mA) is reached.

The dynamics change dramatically with applied field direction. In Fig. 4(a) is a two-dimensional plot showing f as a function of I for the device discussed above, but

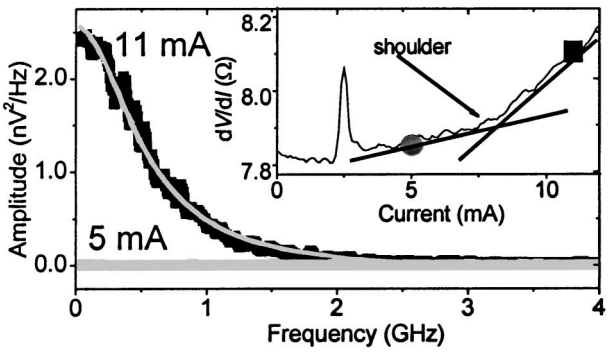

FIG. 3. Low-frequency power spectra for two different currents along with a fit to the data at $I = 11$ mA to a Lorentzian function. The fitted center frequency is $f_0 = 0 \pm 50$ MHz. (inset) The corresponding dV/dI curve.

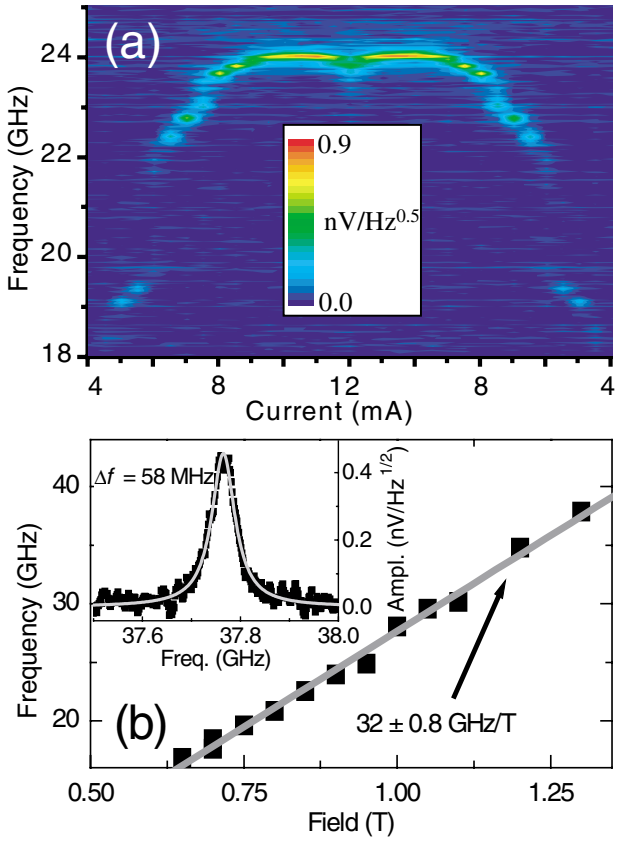

FIG. 4 (color). (a) Plot of f vs I with amplitude shown in a linear color scale from 0 (blue) to 0.9 nV/Hz$^{1/2}$ (red), discretization results from measuring spectra in 500 μA intervals. (b) Out-of-plane f vs H dispersion curve. Data correspond to the highest f at a given H. Error bars (FWHM) are smaller than the data points. (inset) Spectral peak at 1.3 T and $I =$ 11 mA along with a fit.

with an out-of-plane field of 0.9 T. Along the x axis I varies from 4 to 12 mA and back to 4 mA. A vertical slice through the plot yields a frequency spectrum at a fixed I. This field aligns the $Ni_{80}Fe_{20}$ layer with H while canting the $Co_{90}Fe_{10}$ layer about 30° out of the film plane. For $\mu_0 H > 0.6$ T, a blueshift in f with increasing I is seen. More complicated behavior is also found, e.g., jumps in f occur at $I = 6$ mA and 7.5 mA. These jumps are not hysteretic and occur in all devices for out-of-plane fields. According to our modeling of this geometry, the $Ni_{80}Fe_{20}$ magnetization precesses in a nearly circular orbit about H, with frequency increasing with I, the trend seen in our measurements. However, abrupt changes of f with increasing I are not found in our modeling.

As shown in Fig. 4(b), dynamics persist to $\mu_0 H =$ 1.3 T and $f = 38$ GHz, and spectrally can be well fit with a Lorentzian function (inset). Even at these frequencies, the voltage (power) linewidths are $\approx$60 MHz (40 MHz), and have $Q > 650$ (950). Because of bandwidth limitations we were not able to follow the oscillations to higher frequencies. At least for point contacts, the two-state switching behavior found with in-plane fields is largely suppressed in this geometry. As seen in Fig. 4(b), the highest frequencies at a given field vary linearly in H with a slope of 32 GHz/T and give $g =$ 2.1 ± 0.01, differing from the value determined from the in-plane measurements. It may be that H is not yet large enough for f to be a truly linear function of H, leading to an inflated value of g. Finally, in contrast with FMR measurements, we note the excited frequencies here increase continuously in fields ranging from $H < M_{\mathrm{NiFe}}$ to $H > M_{\mathrm{NiFe}}$, and persist even for $H = M_{\mathrm{NiFe}}$ when the FMR resonance frequency is nominally zero.

We thank J. A. Katine for supplying nanopillar devices, and M. D. Stiles and F. B. Mancoff for helpful discussions. This work was supported by the DARPA SPinS and NIST Nano-magnetodynamics programs.

[1] J. C. Slonczewski, J. Magn. Magn. Mater. **159**, L1 (1996); **195**, L261 (1999).
[2] L. Berger, Phys. Rev. B **54**, 9353 (1996).
[3] M. D. Stiles and A. Zangwill, Phys. Rev. B **66**, 014407 (2002); Ya. B. Bazaliy, B. A. Jones, and S. C. Zhang, J. Appl. Phys. **89**, 6793 (2001); S. Zhang, P. M. Levy, and A. Fert, Phys. Rev. Lett. **88**, 236601 (2002); C. Heide, P. E. Zilberman, and R. J. Elliott, Phys. Rev. B **63**, 064424 (2001); X. Waintal *et al.*, Phys. Rev. B **62**, 12 317 (2000).
[4] J. A. Katine *et al.*, Phys. Rev. Lett. **84**, 3149 (2000); E. B. Myers *et al.*, Science **285**, 867 (1999); F. B. Mancoff *et al.*, Appl. Phys. Lett. **83**, 1596 (2003); J.-E. Wegrowe *et al.*, Phys. Lett. **80**, 3775 (2002); J. Grollier *et al.*, Appl. Phys. Lett. **78**, 3663 (2001); J. Z. Sun *et al.*, Appl. Phys. Lett. **81**, 2202 (2002); B. Özyilmaz *et al.*, Phys. Rev. Lett. **91**, 067203 (2003); W. H. Rippard, M. R. Pufall, and T. J. Silva, Appl. Phys. Lett. **82**, 1260 (2003); Y. Ji, C. L. Chien, and M. D. Stiles, Phys. Rev. Lett. **90**, 106601 (2003); S. M. Rezende *et al.*, Phys. Rev. Lett. **84**, 4212 (2000).
[5] S. Urazhdin *et al.*, Phys. Rev. Lett. **91**, 146803 (2003).
[6] J. C. Slonczewski, U.S. Patent No. 5695864, 1997.
[7] S. I. Kiselev *et al.*, Nature (London) **425**, 308 (2003).
[8] M. Tsoi *et al.*, Phys. Rev. Lett. **80**, 4281 (1998); M. Tsoi *et al.*, Nature (London) **406**, 46 (2000).
[9] M. R. Pufall, W. H. Rippard, and T. J. Silva, Appl. Phys. Lett. **83**, 323 (2003).
[10] W. F. Brown, Phys. Rev. **130**, 1677 (1963); Jian-Gang Zhu, J. Appl. Phys. **91**, 7273 (2002).
[11] V. Kambersky and C. E. Patton, Phys. Rev. B **11**, 2668 (1975).
[12] J. P. Nibarger, R. Lopusnik, and T. J. Silva, Appl. Phys. Lett. **82**, 2112 (2003).
[13] S. Kaka *et al.*, J. Appl. Phys. **93**, 7539 (2003); R. H. Koch *et al.*, Phys. Rev. Lett. **81**, 4512 (1998).
[14] Charles Kittel, *Introduction to Solid State Physics* (John Wiley, New York, 1986), 6th ed., p. 454.
[15] G. Wexler, Proc. Phys. Soc. London **89**, 927 (1966).
[16] S. Machlup, J. Appl. Phys. **25**, 341 (1954).